Online Phase-Noise Estimation in FMCW Radar Transceivers Using an Artificial On-Chip Target

Alexander Melzer, *Graduate Student Member, IEEE*, Alexander Onic, *Member, IEEE*, and Mario Huemer, *Senior Member, IEEE*

***Abstract*— The presence of phase noise (PN) severely deteriorates the sensitivity and range of frequency-modulated continuous wave radar systems. Thus, characterization and continuous monitoring of the PN is indispensable, and its estimation is often employed directly on chip. Although many contributions investigate methods for PN estimation, almost all of them consider a continuous-wave (CW) input signal. Differently, in this paper, we aim to estimate the PN from a linear frequency modulated continuous wave (FMCW) signal. For that, we propose two methods utilizing a so-called artificial on-chip target and further digital signal processing. These methods are evaluated in real-time and are the first-known solutions to determine PN estimates during the operation of an FMCW radar transceiver. We prove our methods with both simulation and measurement results from a hardware prototype. Further, we present techniques to efficiently realize the concepts in digital hardware. Finally, we compare and trade off the proposed methods against computational complexity and performance. The novel techniques may be applied to arbitrary input frequencies and bandwidths, and do not require a reference-clock input.**

***Index Terms*— Delay lines, estimation, millimeter-wave frequency-modulated continuous wave (FMCW) radar, monolithic microwave integrated circuits, phase noise (PN).**

I. Introduction

PHASE noise (PN) is the main signal distortion present in any practical frequency generating circuit. Specifically, in frequency-modulated continuous-wave (FMCW) radar systems, it determines the accuracy and sensitivity for object detection [1], [2]. The PN of the phase-locked loop (PLL) within a radar chip is typically measured once at production time to guarantee the anticipated performance. However, with temperature variation and aging of the device, it may alter in an unpredictable way. Thus, on-chip PN measurement techniques are developed.

Manuscript received June 22, 2016; revised August 25, 2016; accepted September 17, 2016. Date of publication November 2, 2016; date of current version December 7, 2016. This work was supported by the Linz Center of Mechatronics (LCM) GmbH as part of a K2 Project. K2 projects are financed using funding from the Austrian COMET K2 program. The COMET K2 projects at LCM are supported by the Austrian Federal Government, the Federal State of Upper Austria, the Johannes Kepler University, and all of the scientific partners which form part of the COMET K2 Consortium. An earlier version of this paper was presented at the 2016 International Microwave Symposium, San Francisco, CA, May 22–27, 2016.

A. Melzer and M. Huemer are with the Institute of Signal Processing, Johannes Kepler University Linz, 4040 Linz, Austria (e-mail: alexander.melzer@jku.at; mario.huemer@jku.at).

A. Onic is with Danube Integrated Circuit Engineering GmbH & Co KG, 4040 Linz, Austria (e-mail: alexander.onic@infineon.com).

Color versions of one or more of the figures in this paper are available online at http://ieeexplore.ieee.org.

Digital Object Identifier 10.1109/TMTT.2016.2614808

Existing on-chip PN estimation concepts rely on a reference clock and a phase frequency detector [3], [4]. Differently, Ishida *et al.* [5] propose a jitter-measurement technique without the need of a reference-clock input. A phase-shifterless version of the delay-line discriminator (DLD) method is proposed in [6]. Although PN estimation techniques have, for example, also been proposed for orthogonal frequency-division multiplexing systems [7], [8], the majority of these techniques constrain the input signal to be a continuous-wave (CW) signal. Hence, those techniques are not applicable to chirp signals used in FMCW radar systems.

In this paper, we aim to estimate the PN power spectrum from a linear FMCW input signal. For that, we utilize the artificial on-chip target (OCT) proposed in [9]. Similar to the DLD method often used for the spectral estimation of PN, the on-chip target (OCT) makes use of a delay line. However, due to the frequency-modulated input signal, the constant 90° phase shift at the phase detector required by the DLD method is no longer ensured. Thus, this technique is inappropriate for an FMCW scheme.

We overcome this issue by employing the OCT and digital signal processing, carried out with a downconverted and low-pass filtered version of the OCT output signal. We propose two different methods to obtain accurate estimates of the PN power spectral density (PSD).

In the first approach, the *residual PN* of the downconverted and low-pass filtered OCT signal is extracted. With its PSD and a frequency-dependent scaling function, the *actual PN* PSD is obtained. This first estimation technique will be referred to as PN estimation in time domain (EMT). The second approach computes the PSD of the downconverted and low-pass filtered OCT signal directly. Through time- and frequency-dependent correction terms, it is converted into the desired PN PSD. The second estimation technique will be referred to as PN estimation in frequency domain (EMF).

Both proposed concepts allow for continuous PN estimation during normal operation of the radar device. Furthermore, without requiring additional measurement equipment, the PN can be measured after production as part of the characterization procedure.

This paper is an extended version of [10]. Therein, we provided the theory of the two PN estimation techniques at a glance together with measurement results. In this paper, we provide in-depth derivations, propose efficient techniques how to compute the estimates in digital hardware, compare their

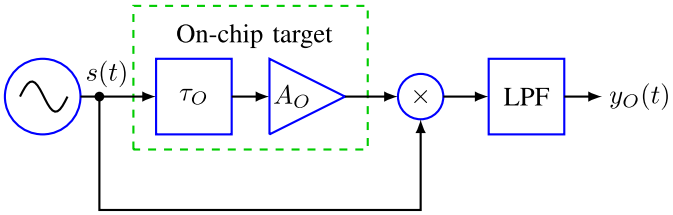

Fig. 1. OCT signal path.

computational complexity, and provide additional simulation and measurement results. For the derivation of the second estimation technique, we further investigate a more general estimation problem and propose a simple yet effective solution to it.

This paper is structured as follows. Section II introduces the system model with the OCT. Section III proposes the first PN estimation technique mainly performed in time domain (EMT). Based on a more generalized estimation problem investigated in Section IV, the second PN estimation technique (EMF), carried out holistically in frequency domain, is proposed in Section V. The two approaches are compared in Section VI with respect to their computational complexity. After proposing our hardware setup for verification in Section VII, simulation and measurement results are presented in Section VIII together with an in-depth analysis. Finally, Section IX provides a discussion and comparison to the existing work.

II. System Model

A. Derivation of the OCT Intermediate Frequency Signal

The system model with the artificial OCT is shown in Fig. 1 and described in the following. The linear FMCW signal generated by a PLL is determined as

$$s(t) = A\cos(2\pi f_0 t + \pi k t^2 + \Phi + \varphi(t)) \tag{1}$$

for $t \in [0, T]$, with the chirp duration T. Further, A is the transmit amplitude, f_0 is the chirp start frequency, k is the chirp slope, Φ is a constant initial phase, and $\varphi(t)$ models the PN. The transmit signal $s(t)$ is fed into the OCT, which applies delay and gain of τ_O and A_O, respectively. Multiplying the OCT output with the instantaneous transmit signal and subsequent low-pass filtering yields the OCT intermediate frequency (IF) signal as

$$\begin{aligned} y_O(t) &= [A_O s(t) s(t-\tau_O)] * h_L(t) \qquad (2)\\ &= \left[\frac{A^2 A_O}{2}\cos(2\pi f_{BO} t + \Phi_O + \Delta\varphi_O(t))\right] * h_L(t) \qquad (3)\end{aligned}$$

where $*$ denotes the convolution operator and $h_L(t)$ is the impulse response of a low-pass filter (LPF) (ideally assumed), eliminating the image from the mixing process. Further, denoting B as the chirp bandwidth, the beat frequency is identified as

$$f_{BO} = k\tau_O = \frac{B}{T}\tau_O \tag{4}$$

and the constant phase is

$$\Phi_O = 2\pi f_0 \tau_O - \pi k \tau_O^2. \tag{5}$$

Without loss of generality, the bypass path in the block diagram in Fig. 1, which directly feeds the mixer, is assumed with zero delay.

B. Low-Pass Filtered Decorrelated Phase Noise

The last signal in (3), $\Delta\varphi_O(t)$, is of particular significance. It is the so-called decorrelated phase noise (DPN) defined as the difference between the instantaneous PN and the PN delayed by τ_O, that is, $\Delta\varphi_O(t) = \varphi(t) - \varphi(t-\tau_O)$. To further analyze the DPN, we rewrite (3) as

$$\begin{aligned} y_O(t) = \Bigg[&\frac{A^2 A_O}{2}\cos(2\pi f_{BO} t + \Phi_O)\cos(\Delta\varphi_O(t)) \\ &- \frac{A^2 A_O}{2}\sin(2\pi f_{BO} t + \Phi_O)\sin(\Delta\varphi_O(t))\Bigg] * h_L(t). \end{aligned} \tag{6}$$

Since $\Delta\varphi_O(t)$ is assumed to be sufficiently small, we can approximate $\cos(\Delta\varphi_O(t)) \approx 1$ and $\sin(\Delta\varphi_O(t)) \approx \Delta\varphi_O(t)$, and thus

$$\begin{aligned} y_O(t) \approx &\frac{A^2 A_O}{2}\cos(2\pi f_{BO} t + \Phi_O) \\ &- \frac{A^2 A_O}{2}\sin(2\pi f_{BO} t + \Phi_O)\Delta\varphi_{OL}(t). \end{aligned} \tag{7}$$

Note that in this approximation, the random phase $\Delta\varphi_O(t)$ is converted into a random amplitude, and is thus affected by the low-pass filtering. This low-pass filtered DPN can be written as

$$\begin{aligned} \Delta\varphi_{OL}(t) &= \Delta\varphi_O(t) * h_L(t) \\ &= [\varphi(t) - \varphi(t-\tau_O)] * h_L(t). \end{aligned} \tag{8}$$

In this paper, we aim to estimate the PN PSD from the DPN $\Delta\varphi_{OL}(t)$, which is contained in the (measurable) OCT IF signal $y_O(t)$. To highlight the particular issue of this estimation problem, we give an example of an FMCW radar system with the state-of-the-art parameters for an automotive application first.

C. Estimation Constraints by Application

In this example, we assume a chirp bandwidth of $B = 1$ GHz and a chirp duration of $T = 100$ μs. Further, consider an economically realizable delay for the OCT with $\tau_O = 200$ ps [11]. From (4), the resulting beat frequency becomes $f_{BO} = 2$ kHz, and thus, for this example, only a fifth of a full period of the term $\sin(2\pi f_{BO} t + \Phi_O)$ in (7) is evaluated during the whole chirp duration T. In other words, only an excerpt of one period of a cyclostationary random signal is observed.

Despite this constraint, we show that the PN PSD of the PLL can be estimated from the OCT IF signal. In Sections III and V, we propose two methods to obtain such estimates based on the presented system model of the OCT.

III. Phase-Noise Estimation From Extracted DPN of OCT IF Signal (EMT)

In this first approach, the PN PSD estimation is carried out mainly in time domain. Still, for completeness, we evaluate some spectral properties of the DPN first.

A. Spectral Properties of Decorrelated Phase Noise

The autocovariance function of the low-pass filtered DPN having zero mean is given as

$$c_{\Delta\varphi_{OL}\Delta\varphi_{OL}}(u) = E\{\Delta\varphi_{OL}(t)\Delta\varphi_{OL}(t+u)\}. \tag{9}$$

On the other hand, from (8) and the Wiener–Lee relation, we readily have that

$$c_{\Delta\varphi_{OL}\Delta\varphi_{OL}}(u) = c_{\Delta\varphi_O\Delta\varphi_O}(u) * c_{hh}(u). \tag{10}$$

Therein, $c_{\Delta\varphi_O\Delta\varphi_O}(u)$ and $c_{hh}(u)$ are the autocovariance function of $\Delta\varphi_O(t)$ and the energy autocorrelation function of the LPF impulse response $h_L(t)$, respectively. For $c_{\Delta\varphi_O\Delta\varphi_O}(u)$, we further have

$$\begin{aligned} c_{\Delta\varphi_O\Delta\varphi_O}(u) &= E\{\Delta\varphi_O(t)\Delta\varphi_O(t+u)\} \\ &= E\{\varphi(t)\varphi(t+u)\} - E\{\varphi(t)\varphi(t+u-\tau_O)\} \\ &\quad - E\{\varphi(t-\tau_O)\varphi(t+u)\} \\ &\quad + E\{\varphi(t-\tau_O)\varphi(t+u-\tau_O)\}. \end{aligned} \tag{11}$$

Plugging in the autocovariance function of the PN, which is $c_{\varphi\varphi}(u) = E\{\varphi(t)\varphi(t+u)\}$, (11) can be rewritten as

$$c_{\Delta\varphi_O\Delta\varphi_O}(u) = 2c_{\varphi\varphi}(u) - c_{\varphi\varphi}(u-\tau_O) - c_{\varphi\varphi}(u+\tau_O). \tag{12}$$

Then, with the Wiener–Khintchine theorem, the PSD of the DPN is determined as

$$\begin{aligned} S_{\Delta\varphi_O\Delta\varphi_O}(f) &= \mathcal{F}\{c_{\Delta\varphi_O\Delta\varphi_O}(u)\} \\ &= 2S_{\varphi\varphi}(f) - S_{\varphi\varphi}(f)(e^{j2\pi f\tau_O} + e^{-j2\pi f\tau_O}) \\ &= 2S_{\varphi\varphi}(f)(1-\cos(2\pi f\tau_O)) \end{aligned} \tag{13}$$

where $\mathcal{F}$ denotes the Fourier transform. This result is also described in [12].

For the low-pass filtered DPN, we have from (10) that

$$S_{\Delta\varphi_{OL}\Delta\varphi_{OL}}(f) = S_{\Delta\varphi_O\Delta\varphi_O}(f)|H_L(f)|^2 \tag{14}$$

where $|H_L(f)|$ is the magnitude response of the LPF. Plugging in (13), the PSD of the low-pass filtered DPN $S_{\Delta\varphi_{OL}\Delta\varphi_{OL}}(f)$ evaluates to

$$S_{\Delta\varphi_{OL}\Delta\varphi_{OL}}(f) = 2S_{\varphi\varphi}(f)|H_L(f)|^2(1-\cos(2\pi f\tau_O)). \tag{15}$$

B. Extraction of the Decorrelated Phase Noise

In (15) we developed a relation between the desired PN PSD and the PSD of the DPN $\Delta\varphi_{OL}(t)$. To obtain the latter we now extract the DPN in time domain from the OCT IF signal $y_O(t)$, which we will obtain later on from a sampling device in discrete time. By rearranging (7), the DPN is readily extracted as

$$\Delta\varphi_{OL}(t) \approx \frac{\frac{A^2A_O}{2}\cos(2\pi f_{BO}t + \Phi_O) - y_O(t)}{\frac{A^2A_O}{2}\sin(2\pi f_{BO}t + \Phi_O)}. \tag{16}$$

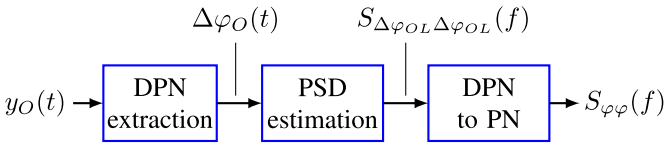

Fig. 2. PN estimation from extracted DPN.

In (16), the denominator has zeros depending on f_{BO} and Φ_O. These two parameters are adjusted with the sweep slope k and the OCT delay τ_O. The latter is a design parameter, and can, thus, be chosen to avoid the denominator in (16) to become zero within the duration of a chirp. In [11], we propose how to optimally choose the delay τ_O, such that the ratio between the power of the DPN and the intrinsic noise contained within $y_O(t)$ is maximized.

C. Phase-Noise Estimation

By rearranging (15), we can readily express the PN PSD as

$$S_{\varphi\varphi}(f) = \frac{S_{\Delta\varphi_{OL}\Delta\varphi_{OL}}(f)}{2|H_L(f)|^2(1-\cos(2\pi f\tau_O))}. \tag{17}$$

This identity relates the PSD of the DPN to that of the PN. With the known design parameters A, A_O, and τ_O, $S_{\Delta\varphi_{OL}\Delta\varphi_{OL}}(f)$ can be obtained by applying a state-of-the-art PSD estimation of the sampled version of $\Delta\varphi_{OL}(t)$ in (16), and subsequently, the desired PN PSD can be derived from (17).

At this point, it is important to note that the correction by $|H_L(f)|^2$ above the cutoff frequency is of theoretical interest only. The PSD estimate $S_{\Delta\varphi_{OL}\Delta\varphi_{OL}}(f)$ will be valid only up to the cutoff frequency of the LPF in a real-world application. For higher frequencies, the measurement noise will dominate.

The PN estimation procedure is summarized in the block diagram in Fig. 2. First, the DPN $\Delta\varphi_{OL}(t)$ is extracted from the OCT IF signal according to (16). Second, the DPN PSD $S_{\Delta\varphi_{OL}\Delta\varphi_{OL}}(f)$ is estimated. Third, this PSD is converted into the desired PN power spectrum with the identity from (17). In the sequel, a practical estimation approach for this technique is investigated.

D. Practical Estimation Approach

In practice, the OCT IF signal is sampled by an analog to digital converter (ADC). The extracted DPN from the digitized OCT IF signal is, based on (16), obtained as

$$\Delta\varphi_{OL}[n] \approx \frac{\frac{A^2A_O}{2}\cos(2\pi f_{BO}nT_s + \Phi_O) - y_O[n]}{\frac{A^2A_O}{2}\sin(2\pi f_{BO}nT_s + \Phi_O)} \tag{18}$$

where T_s is the sampling interval and $y_O[n]$ is the sampled OCT IF signal. We consider the circuit design parameters A, A_O, and τ_O to be known. Thus, also the beat frequency f_{BO} and the constant phase Φ_O can be determined from (4) and (5), respectively.

To estimate the PSD of $\Delta\varphi_{OL}[n]$, we use Welch's method. Although it is a well-known technique, we introduce it briefly, such that the notation and differences to EMF can be drawn later on. We split $\Delta\varphi_{OL}[n]$ into I overlapping segments of

length M as $\Delta\varphi_{OL}^{(i)}[n] = \Delta\varphi_{OL}[n + iD]$, $n = 0, \ldots, M-1$, $i = 0, \ldots, I-1$, where D defines the respective offset and, thus, the overlap between the segments. Then, with Welch's method, we have

$$\hat{S}_{\Delta\varphi_{OL}\Delta\varphi_{OL}}[k] = \frac{1}{I}\sum_{i=0}^{I-1} \hat{S}^{(i)}_{\Delta\varphi_{OL}\Delta\varphi_{OL}}[k] \tag{19}$$

where the ith segment is computed as

$$\hat{S}^{(i)}_{\Delta\varphi_{OL}\Delta\varphi_{OL}}[k] = \frac{1}{MU}\left|\sum_{n=0}^{M-1} \Delta\varphi_{OL}^{(i)}[n] w_M[n] e^{-j\frac{2\pi k}{M}n}\right|^2. \tag{20}$$

Therein, k is the discrete frequency index, and $w_M[n]$ is the applied window function, having length M and average power U. Finally, with the result from (17), the PN PSD becomes

$$\hat{S}_{\varphi\varphi}[k] = \frac{\hat{S}_{\Delta\varphi_{OL}\Delta\varphi_{OL}}[k]}{2|H_L[k]|^2(1-\cos(2\pi k/Mf_s\tau_O))} \tag{21}$$

where f_s is the sampling frequency. Note that we use round brackets to indicate analog, continuous time PSDs of random signals, for instance, $S_{\varphi\varphi}(f)$. For PSDs of sampled, discrete time signals, we use square brackets, for instance, $\hat{S}_{\varphi\varphi}[k]$. Thus, to obtain a sampled version of the analog PSD $S_{\varphi\varphi}(f)$ from $\hat{S}_{\varphi\varphi}[k]$, a scaling by T_s is required.

The PSD estimate from (19) can be computed efficiently using the fast Fourier transform (FFT) in (20). Nevertheless, EMT requires additional computation steps that can be avoided. Hence, we will present a method to estimate the PN PSD, which does not require this extraction process. It is determined holistically in the frequency domain. Prior to formulating this method in Section V, we investigate a more generalized estimation problem in Section IV.

IV. Spectral Estimation of Modulated Band-Limited Noise

In this section, we consider a more generalized estimation problem. The result will be applied to the second method to estimate the PN (EMF) in FMCW radars using the artificial OCT later on in Section V.

For now, we aim to estimate the PSD $S_{ww}(f)$ of band-limited, stationary, and ergodic noise $w(t)$ modulated by a (slow) time limited sinusoidal as

$$x(t) = A_x \sin(2\pi f_x t + \Phi_x) w(t) \tag{22}$$

where A_x is some amplitude, f_x is the frequency, Φ_x is a constant phase, and $w(t)$ is zero mean stationary and ergodic band-limited noise. The estimation shall be performed solely in frequency domain. We assume A_x, f_x and Φ_x to be known.

Note that through the multiplication of the stationary $w(t)$ with an infinite length sinusoid, the resulting random signal would become cyclostationary. However, according to our assumptions, (22) is evaluated for $t \in [0, T]$, with $T < T_x = 1/f_x$. Thus, $x(t)$ is just an excerpt of a cyclostationary random signal. This particular estimation problem is not found in the standard literature.

A. Spectral Estimation

In order to solve the estimation problem at hand, the PSD of (22) is computed first. The autocovariance function of $x(t)$ is determined as

$$\begin{aligned} c_{xx}(t,u) &= E\{x(t)x(t+u)\} \\ &= \frac{A_x^2}{4j^2}E \\ &\quad \times \{[e^{j(2\pi f_x t+\Phi_x)} - e^{-j(2\pi f_x t+\Phi_x)}]w(t) \\ &\quad \cdot [e^{j(2\pi f_x (t+u)+\Phi_x)} - e^{-j(2\pi f_x (t+u)+\Phi_x)}]w(t+u)\} \\ &= \frac{A_x^2}{4}c_{ww}(u)[e^{j2\pi f_x u} + e^{-j2\pi f_x u} - e^{j(4\pi f_x t+2\Phi_x)}e^{j2\pi f_x u} \\ &\quad - e^{-j(4\pi f_x t+2\Phi_x)}e^{-j2\pi f_x u}] \end{aligned} \tag{23}$$

where $c_{ww}(u)$ is the autocovariance function of the noise $w(t)$. Note that within the last two summands in the last step, the terms $e^{\pm j(4\pi f_x t+2\Phi_x)}$ do not depend on u. To obtain the (time variant) PSD of $x(t)$, we compute the Fourier transform of (23), which is

$$\begin{aligned} S_{xx}(f,t) = \frac{A_x^2}{4}[&S_{ww}(f-f_x) + S_{ww}(f+f_x) \\ &- S_{ww}(f-f_x)e^{j(4\pi f_x t+2\Phi_x)} \\ &- S_{ww}(f+f_x)e^{-j(4\pi f_x t+2\Phi_x)}]. \end{aligned} \tag{24}$$

To further simplify this equation, we assume the frequency f_x to be negligibly small. This assumption will also hold true for our particular application of estimating the PN in an FMCW transceiver. We therefore approximate

$$S_{ww}(f) \approx S_{ww}(f-f_x) \approx S_{ww}(f+f_x) \tag{25}$$

and thus

$$\begin{aligned} S_{xx}(f,t) &\approx \frac{A_x^2}{4}[2S_{ww}(f) - 2S_{ww}(f)\cos(4\pi f_x t + 2\Phi_x)] \\ &= \frac{A_x^2}{2}S_{ww}(f)\gamma_x(t) \end{aligned} \tag{26}$$

with the correction term

$$\gamma_x(t) = 1 - \cos(4\pi f_x t + 2\Phi_x) \tag{27}$$

which is evaluated for $t \in [0, T]$. Finally, solving (26) for $S_{ww}(f)$ yields

$$S_{ww}(f) \approx \frac{2S_{xx}(f,t)}{A_x^2\gamma_x(t)}. \tag{28}$$

It is important to note that $S_{ww}(f)$, the PSD of a stationary random process, is obtained from the PSD of the excerpt of a cyclostationary signal. To compensate for this cyclostationarity, and thus for the time dependence within $S_{xx}(f,t)$, the correction term $\gamma_x(t)$ is applied. However, in practice, it is not feasible to obtain the PSD $S_{xx}(f,t)$ for every time t, which could theoretically be obtained from an ensemble average of a statistically sufficient amount of realizations of $x(t)$. We therefore seek for a practically feasible way to evaluate (28).

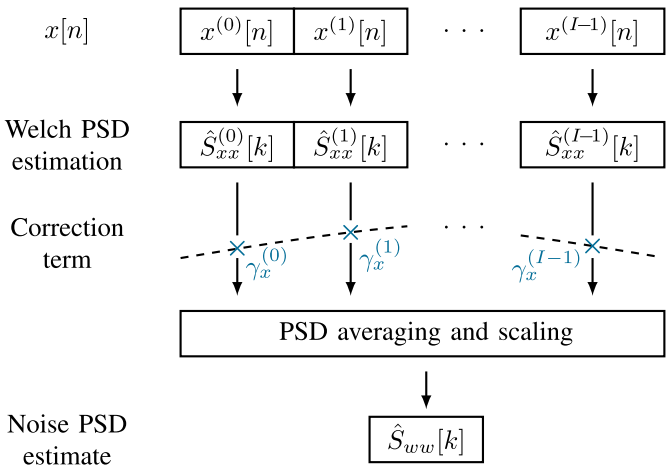

Fig. 3. Schematic of the estimation procedure. For better visualization, no overlap ($D = M$) is assumed.

B. Practical Estimation Approach

The discrete time version of $x(t)$ in (22) is given as

$$x[n] = A_x \sin(2\pi f_x n T_s + \Phi_x) w[n] \tag{29}$$

where n is the discrete time index and T_s is the sampling interval. The noise is assumed to be band-limited such that aliasing is avoided.

To estimate the PSD of $x[n]$, it is split into I overlapping segments of length M with $x^{(i)}[n] = x[n + iD]$ as carried out in Section III-D as well. According to Welch's method, each segment is multiplied with a window function $w_M[n]$ before the PSD of the segment is computed using the FFT. To compensate for the nonstationarity of $x[n]$, we scale each segment with the correction term introduced in (27). Hence, based on (28), the PSD estimate of $w[n]$ evaluates to

$$\hat{S}_{ww}[k] = \frac{2}{I A_x^2} \sum_{i=0}^{I-1} \frac{\hat{S}_{xx}^{(i)}[k]}{\gamma_x^{(i)}} \tag{30}$$

with the PSD of the ith segment

$$\hat{S}_{xx}^{(i)}[k] = \frac{1}{MU} \left| \sum_{n=0}^{M-1} x^{(i)}[n] w_M[n] e^{-j\frac{2\pi k}{M} n} \right|^2. \tag{31}$$

Further, the correction term is

$$\gamma_x^{(i)} = 1 - \cos\left[4\pi f_x \left(iD + \frac{M-1}{2} \right) T_s + 2\Phi_x \right] \tag{32}$$

which is evaluated at the center of the window of the ith segment.

Note again that due to the scaling with $\gamma_x^{(i)}$, the nonstationarity of $x[n]$ is compensated. Thus, the segments can be averaged and also the time index i omitted on the left-hand side of (30). The smaller the segment length is chosen, the more accurate the correction is.

The overall estimation procedure is schematically represented in Fig. 3 with no overlap of the segments for better visualization. From a computational complexity point of view, it is interesting to note that the Welch estimate is simply extended by the scaling with $\gamma_x^{(i)}$. Hence, computation of the PSD in (30) comes with almost no additional complexity compared with a conventional Welch PSD estimation.

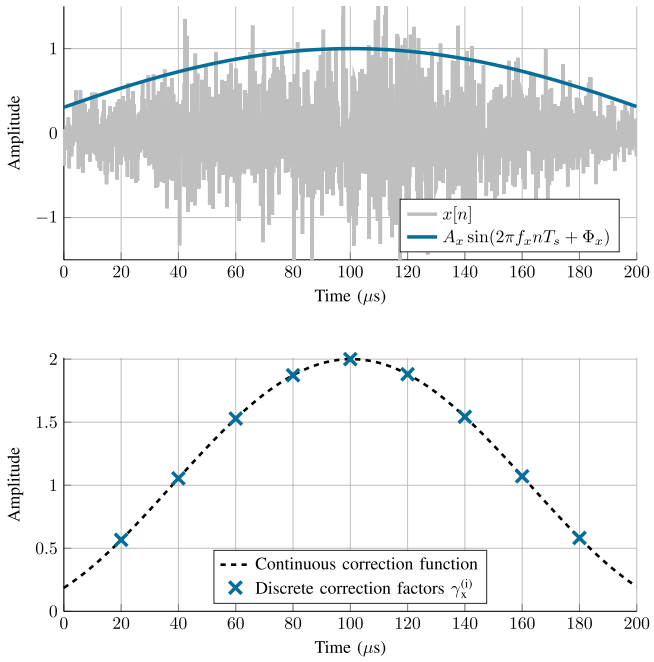

Fig. 4. Top: exemplary modulated WGN signal as well as the sinusoidal without noise. Bottom: continuous correction function together with discrete correction terms $\gamma_x^{(i)}$.

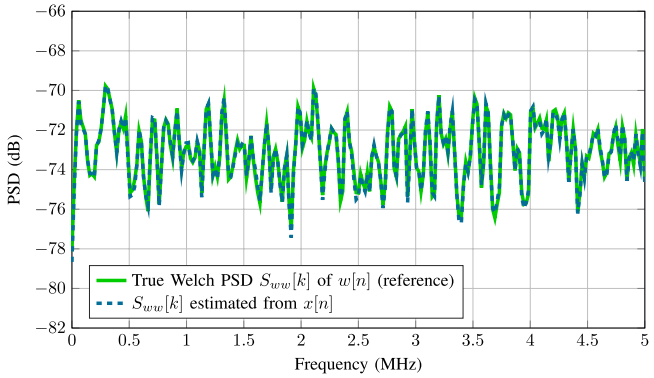

Fig. 5. Directly estimated PSD from $w[n]$, and the same estimated from $x[n]$.

C. Example

Consider an example with $A_x = 1$, $f_x = 2$ kHz, and $\Phi_x = 0.31$. The noise $w[n]$ is WGN with zero mean and variance $\sigma_w^2 = 0.25$. Evaluating $x[n]$ from (29) for $n \in \{0, 1, \ldots, 1999\}$ with $f_s = 1/T_s = 10$ MHz yields the signal depicted in Fig. 4 (top).

For the PSD estimation, we use $M = 400$ and $D = 200$. The resulting continuous correction function as well as the discrete correction terms $\gamma_x^{(i)}$ are depicted in Fig. 4 (bottom). The estimated PSD of $w[n]$ with the proposed method is depicted in Fig. 5. As a reference, the true Welch PSD from $w[n]$ is provided.

It can be seen that the estimate delivers an almost perfect match to the reference. A slight estimation error occurs due to

the approximation in (25). Further, also the segment length M determines the estimation accuracy. It decreases with increasing M as a single correction value $\gamma_x^{(i)}$ is used for scaling of the PSD estimate of one segment.

D. Discussion

In this section, a new technique for the estimation of the average PSD of a cyclostationary random process, which is observable for an excerpt of its period only, was derived. A different and more general version of this estimation problem is often found in practice, when a sufficiently long sequence of the signal can be observed. Then, the PSD estimation is carried out over several periods of the cyclostationary process. As an example, for pulse amplitude modulated (PAM) signals in communications, one or more full symbol periods are typically regarded to estimate their PSD [13]. In such cases, also phase-randomization procedures are applied to obtain a PSD describing the average behavior [14].

Anyhow, it is important to note that, with a proper signal model at hand, our estimation technique may be applied also in other fields. For instance, in audio signal processing, where, for simplification, speech is often assumed to be short-term stationary, our technique may yield improved results for spectral estimation [15]. In the sequel, the proposed estimation technique will be applied to the PN estimation problem at hand.

V. Phase-Noise Estimation from On-Chip Target IF Signal (EMF)

With the findings of the previous section, we now propose a second approach to perform the PN PSD estimation. This approach performs the estimation solely from the PSD of the OCT IF signal. In contrast to EMT, it does not require the DPN extraction process in time domain.

We reconsider the approximation of the OCT IF signal from (7)

$$y_O(t) \approx \underbrace{\frac{A^2 A_O}{2}\cos(2\pi f_{BO} t + \Phi_O)}_{y_{O1}(t)} - \underbrace{\frac{A^2 A_O}{2}\sin(2\pi f_{BO} t + \Phi_O)\Delta\varphi_{OL}(t)}_{y_{O2}(t)}. \quad (33)$$

The signal of interest is the PSD of the PN contained within $\Delta\varphi_{OL}(t)$. To proceed, we compute the PSD of (33). Since the DPN is assumed to have zero mean, the autocovariance function of $y_O(t)$ is

$$c_{y_O y_O}(t,u) = E\{y_O(t) y_O(t+u)\} = \underbrace{y_{O1}(t) y_{O1}(t+u)}_{c_{y_{O1}y_{O1}}(t,u)} + \underbrace{E\{y_{O2}(t) y_{O2}(t+u)\}}_{c_{y_{O2}y_{O2}}(t,u)}. \quad (34)$$

It will become clear later on that the deterministic part $c_{y_{O1}y_{O1}}(t,u)$ immediately follows from the stochastic part $c_{y_{O2}y_{O2}}(t,u)$. Thus, we investigate the latter first.

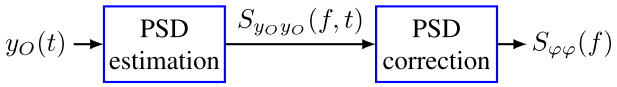

Fig. 6. Direct PN estimation from OCT IF signal in frequency domain.

A. Stochastic Part

The signal $y_{O2}(t)$ represents an excerpt of a cyclostationary random signal, since, in our particular example, (33) is evaluated for $t \in [0, T]$, with $T < 1/f_{BO}$. Nonetheless, to obtain its power spectrum, we may apply the findings from Section IV as $y_{O2}(t)$ is in the form of (22). From (26), its PSD immediately follows to:

$$S_{y_{O2}y_{O2}}(f,t) \approx \frac{(A^2 A_O)^2}{8} S_{\Delta\varphi_{OL}\Delta\varphi_{OL}}(f)\gamma_2(t) \quad (35)$$

with

$$\gamma_2(t) = 1 - \cos(4\pi f_{BO} t + 2\Phi_O). \quad (36)$$

Note that in (35), we used the same approximation as in (25). By further applying (15), (35) evaluates to

$$S_{y_{O2}y_{O2}}(f,t) \approx \frac{(A^2 A_O)^2}{4} S_{\varphi\varphi}(f)|H_L(f)|^2 \cdot [1 - \cos(2\pi f \tau_O)]\,\gamma_2(t) \quad (37)$$

expressing the PN PSD we aim to estimate.

B. Deterministic Part

The deterministic part in (33) is given by $y_{O1}(t)$. With a similar derivation as carried out in Section IV-A, it can be easily shown that the PSD of $y_{O1}(t)$ is

$$S_{y_{O1}y_{O1}}(f,t) \approx \frac{(A^2 A_O)^2}{8}\delta(f)\gamma_1(t) \quad (38)$$

with

$$\gamma_1(t) = [1 + \cos(4\pi f_{BO} t + 2\Phi_O)] \quad (39)$$

and $\delta(\cdot)$ being the Dirac delta function.

C. Phase-Noise Estimation

With the results from the previous sections, we can now determine the PN PSD. Based on (34), we have that

$$S_{y_O y_O}(f,t) = S_{y_{O1}y_{O1}}(f,t) + S_{y_{O2}y_{O2}}(f,t). \quad (40)$$

Finally, with (37), we can express the desired PN PSD as

$$S_{\varphi\varphi}(f) \approx \frac{4[S_{y_O y_O}(f,t) - S_{y_{O1}y_{O1}}(f,t)]}{(A^2 A_O)^2 |H_L(f)|^2 [1 - \cos(2\pi f \tau_O)]\gamma_2(t)}. \quad (41)$$

As indicated, $S_{y_O y_O}(f,t)$ and $S_{y_{O1}y_{O1}}(f,t)$ are time-dependent PSDs. However, equivalent to the earlier discussion, the correction terms $\gamma_1(t)$ and $\gamma_2(t)$ compensate for the nonstationarity.

The simplified estimation procedure is summarized in the block diagram in Fig. 6. First, the PSD of the OCT IF signal $S_{y_O y_O}(f,t)$ is estimated. Second, the time dependence is compensated by the correction terms, and, together with the other manipulations in (41), the desired PN power spectrum is obtained. In the sequel, a practical estimation approach for this technique is investigated.

TABLE I
COMPUTATIONAL COMPLEXITY FOR THE PN ESTIMATION FROM $\Delta\varphi_{OL}(t)$ (EMT) OVER ONE CHIRP

Operation	Multiplications	Additions	ROM bits	Equation(s)
DPN extraction	$\underbrace{T\,f_s}_{\text{CORDIC scaling}} + \underbrace{T\,f_s}_{\text{Div. by }\sin(\cdot)}$	$\underbrace{T\,f_s}_{\cos(\cdot)-y_O[n]} + \underbrace{T\,f_s\,\text{ADD}_{\text{CORDIC}}}_{\text{CORDIC rotation}} + \underbrace{T\,f_s}_{\text{CORDIC phase incr.}}$	0	(18)
PSD estimation	$I\left(\underbrace{M}_{w_M} + \underbrace{4\,M/2\log_2(M)}_{\text{FFT}} + \underbrace{M}_{|\cdot|^2} + 1\right) + 1$	$I\,\underbrace{(2\,M\log_2(M))}_{\text{FFT}}$	$\underbrace{M\,N_b}_{w_M}$	(19), (20)
DPN to PN	M	0	$\underbrace{M\,N_b}_{\text{Denom. of (21)}}$	(21)
Asymptotic complexity	$\mathcal{O}(T\,f_s + IM\log_2(M))$	$\mathcal{O}(T\,f_s + IM\log_2(M))$	$\mathcal{O}(M\,N_b)$	

TABLE II
COMPUTATIONAL COMPLEXITY FOR THE PN ESTIMATION FROM $y_O(t)$ IN THE FREQUENCY DOMAIN (EMF) OVER ONE CHIRP

Operation	Multiplications	Additions	ROM bits	Equation(s)
PSD estimation	$I\left(\underbrace{M}_{w_M} + \underbrace{4\,M/2\log_2(M)}_{\text{FFT}} + \underbrace{M}_{|\cdot|^2} + 1\right) + 1$	$I\,\underbrace{(2\,M\log_2(M))}_{\text{FFT}}$	$\underbrace{M\,N_b}_{w_M}$	(42)
DPN correction	$\underbrace{M}_{\text{Pre-scaling factor in (45)}} + \underbrace{I\,M}_{\gamma_1^{(i)}} + \underbrace{I\,M}_{\gamma_2^{(i)}}$	$\underbrace{I\,M}_{\text{Num. in sum of (45)}}$	$\underbrace{M\,N_b}_{\text{Pre-scaling factor}} + \underbrace{M\,N_b}_{S^{(i)}_{y_{O1}y_{O1},W}[k]} + \underbrace{I\,N_b}_{\gamma_1^{(i)}} + \underbrace{I\,N_b}_{\gamma_2^{(i)}}$	(45)
Asymptotic complexity	$\mathcal{O}(IM\log_2(M))$	$\mathcal{O}(IM\log_2(M))$	$\mathcal{O}((M+I)\,N_b)$	

D. Practical Estimation Approach

To determine the PN, we aim to approximate (41). We start by estimating the PSD of $y_O(t)$, whose discretized signal $y_O[n]$ is retrieved from the ADC. Analogous to the estimation in (31), we split this signal into I overlapping segments of length M with $y_O^{(i)}[n] = y_O[n + i\,D]$ and estimate its PSD using Welch's method as

$$\hat{S}^{(i)}_{y_O y_O}[k] = \frac{1}{MU}\left|\sum_{n=0}^{M-1} y_O^{(i)}[n] w_M[n] e^{-j\frac{2\pi k}{M}n}\right|^2. \tag{42}$$

Next, we compute the deterministic PSD of $y_{O1}[n]$, which can be precomputed. We incorporate the window function through the convolution with the Dirac impulse in (38). In fact, the peak in the power spectrum is spread by the magnitude response $|W_M[k]|$ of the window function as

$$S^{(i)}_{y_{O1}y_{O1},W}[k] = \frac{(A^2 A_O)^2}{8}|W_M[k]|^2 \gamma_1^{(i)}. \tag{43}$$

For example, $|W_M[k]|$ for the often used Hann window is defined in [16]. From (39), the correction term $\gamma_1^{(i)}$ becomes

$$\gamma_1^{(i)} = \left[1 + \cos\left(4\pi f_{BO}\left(i\,D + \frac{M-1}{2}\right)T_s + 2\Phi_O\right)\right] \tag{44}$$

which is evaluated at the center of the window of the ith segment. Clearly, the deterministic PSD $S^{(i)}_{y_{O1}y_{O1},W}[k]$ from (43) can be stored up to the scaling factor $\gamma_1^{(i)}$ in a lookup table with the known design parameters A and A_O.

The final averaging and scaling step to obtain the PN estimate is

$$\hat{S}_{\varphi\varphi}[k] = \frac{4}{I(A^2A_O)^2|H_L[k]|^2\,[1-\cos(2\pi k/Mf_s\tau_O)]} \cdot \sum_{i=0}^{I-1}\frac{\hat{S}^{(i)}_{y_O y_O}[k] - S^{(i)}_{y_{O1}y_{O1},W}[k]}{\gamma_2^{(i)}}. \tag{45}$$

Note once again that we compensate for the nonstationarity by scaling with $\gamma_2^{(i)}$ determined as

$$\gamma_2^{(i)} = \left[1 - \cos\left(4\pi f_{BO}\left(i\,D + \frac{M-1}{2}\right)T_s + 2\Phi_O\right)\right]. \tag{46}$$

Thus, we may average over all I segments and omit the time index i on the left-hand side of (45).

VI. COMPUTATIONAL COMPLEXITY

In Section III and Section V, EMT and EMF have been proposed to obtain PN PSD estimates using the OCT. This section compares the two estimation methods with respect to computational complexity and memory requirements. The analysis is done based on the fundamental operations of EMT and EMF, shown in Figs. 2 and 6, respectively. The required multiplications, additions, as well as ROM bits are provided in Tables I and II for the two algorithms. The amount of required operations and ROM bits for each computation step are determined from the equation(s) that are listed in the rightmost column within the tables. Further, the asymptotic

complexity is given in the last row for each of the tables using the $\mathcal{O}$-Notation.

Since we target a full-custom implementation of our PN estimation techniques in an integrated circuit (IC), we now make a few assumptions about the implementation. These are required in order to be able to analyze and compare them in more detail. For the DPN extraction (EMT), we utilize the coordinate rotation digital computer (CORDIC) algorithm. It is highly beneficial to this purpose, since the arguments within the $\sin(\cdot)$ and $\cos(\cdot)$ terms in (16) are identical. It allows both sinusoids to be retrieved with a single CORDIC instance at every discrete time step. In Table I, $\text{ADD}_{\text{CORDIC}}$ represents the number of additions required for a whole CORDIC rotation. Further, a phase increment is required from outside the CORDIC together with a multiplication for the scaling. The ROM bit width is denoted by N_b. For the analysis carried out in this paper, we assume a CORDIC implementation with 12 iterations and three additions for each microrotation. This results in $\text{ADD}_{\text{CORDIC}} = 36$ additions required for each CORDIC rotation. Finally, note that for computation of the FFT, complex multiplications are required. Even if there is some potential for optimization here, we consider a complex multiplication to be realized with four real multiplications and two additions.

From Tables I and II it can be deduced that the PSD estimation step has equivalent complexity for both EMT and EMF. The essential difference is the DPN extraction in time domain for EMT and the DPN correction in frequency domain for EMF. In contrast to the EMT, the DPN correction is performed fully in the frequency domain within the EMF. Consequently, signal processing is done solely on the M discrete frequency indices rather than at all Tf_s samples in time domain. This becomes particularly obvious by comparing the asymptotic complexity of the two algorithms.

To further evaluate this, we compute the exact computational complexity for varying sampling frequencies f_s, since, as will turn out later on, the sampling frequency is an important parameter for our PN estimation techniques. The chirp duration T is held constant, such that, actually, the number of samples to be processed alters with f_s. For the complexity analysis, we consider an FFT length of $M = 1000$, the segment overlap for the Welch PSD estimation with 50%, and the chirp duration $T = 500\ \mu$s (the same parameters will be used for comparison of simulation and measurement results in Section VIII). Further, the used ROM bit width is $N_b = 16$. The resulting number of multiplications, additions, and ROM bits are shown in Fig. 7. It is observed that the number of multiplications is fairly equal to for both of the algorithms. However, the number of additions and the required memory completely differs. While for EMT the number of additions is almost twice as high as for EMF, it is the other way round for the required memory. However, considering the absolute numbers, overall, we consider EMF to be computationally slightly less expensive than EMT.

VII. Experimental Hardware Setup

In this section, we present our hardware setup, which will be used later on to verify our proposed PN estimation methods.

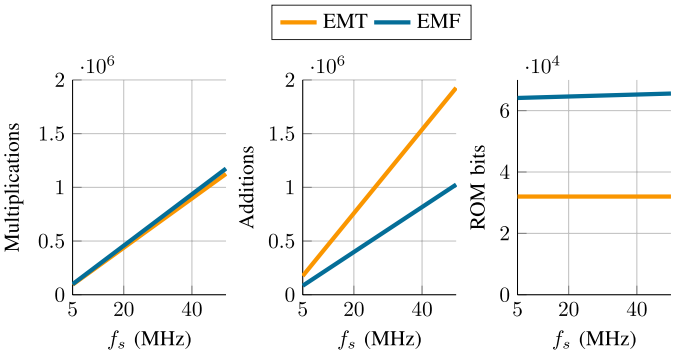

Fig. 7. Computational complexity and memory requirements of EMT and EMF against the sampling frequency f_s.

A block diagram of the hardware setup is provided in Fig. 8. For the generation of the FMCW signal, we utilize the Analog Devices EV-ADF4159EB1Z evaluation board. It integrates the ADF4159 fractional-N frequency synthesizer and a voltage-controlled oscillator (VCO) capable to generate output signals between 11.4 and 12.8 GHz. The chirp parameters (f_0, B, T) are configured through a USB interface. As input to the ADF4159, a $20-$MHz external reference is supplied. The output signal power of the VCO is 3 dBm.

As shown in Fig. 8, the VCO output signal is amplified by a power amplifier (PA) to 18 dBm. This is required, since we use a passive mixer later on. The amplified VCO output signal is then split into two paths with a Wilkinson divider. The first path is fed directly into the local oscillator (LO) port of the passive mixer. The second is fed into the OCT, which is modeled with a coaxial cable. Its output is connected to the radio frequency (RF) port of the passive mixer. The used cable length is 10.2 cm. Together with a relative dielectric constant $\epsilon_r = 2.25$, the delay becomes $\tau_O = 507$ ps. The IF output signal of the mixer is low-pass filtered and sampled with a scope subsequently. The digital signal processing part with the two PN estimation methods is carried out in MATLAB. A picture of the hardware prototype is shown in Fig. 9, and the complete lab setup is presented in Fig. 10.

To measure the reference PN power spectrum, we temporarily configure the ADF4159 to output a continuous wave (CW) signal. Then, we measure the PN PSD with a spectrum analyzer with PN measurement capability. This is indicated by the dashed line in Fig. 8.

VIII. Simulation and Measurement Results

A. System Parameters

The FMCW system parameters are equivalent for both simulations and measurements, and are chosen as follows. The chirp start frequency, bandwidth, and duration are $f_0 = 11.8$ GHz, $B = 200$ MHz, and $T = 500\ \mu$s, respectively. The two PN estimation methods EMT and EMF are applied to the low-pass filtered OCT IF signals (cutoff frequency $f_c = 10$ MHz), which are sampled with $f_s = 20$ MHz. The Welch PSD estimates are carried out with an FFT length of $M = 1000$ and $D = 500$ (50% overlap between the segments). For generation of the PN within the simulation, the reference PN PSD was used. This reference PN was determined as the

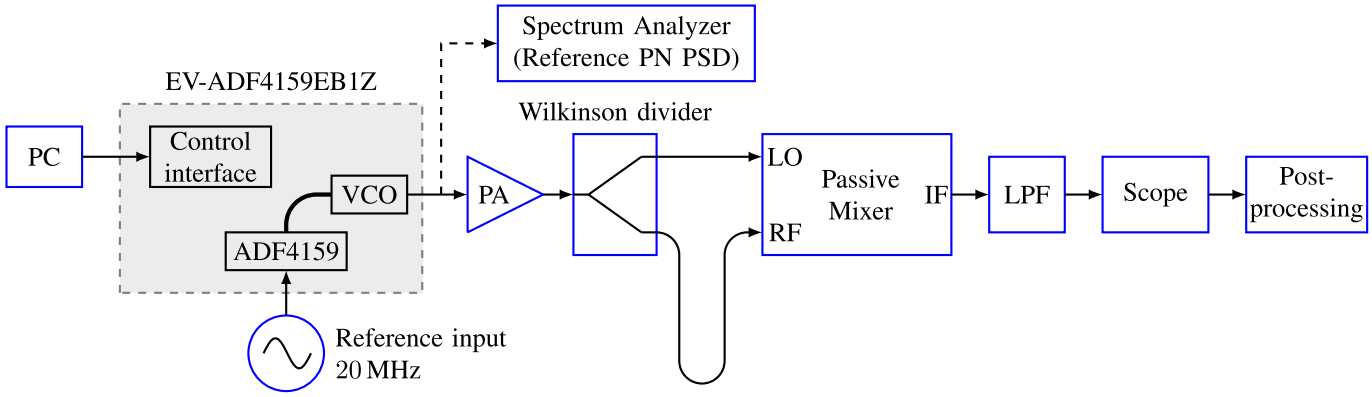

Fig. 8. Block diagram of the experimental hardware setup.

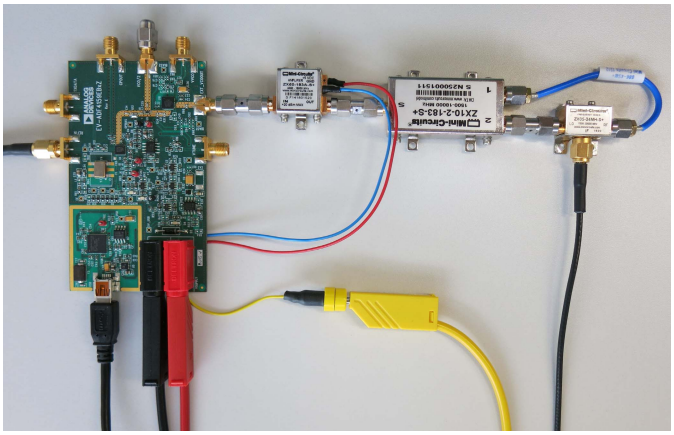

Fig. 9. Photograph of the experimental hardware setup.

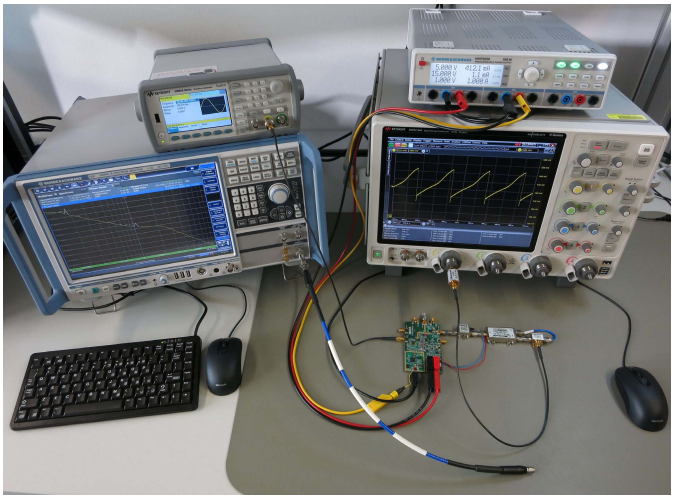

Fig. 10. Lab setup depicting the hardware prototype, the power supply, the signal generator (reference input for the PLL), the spectrum analyzer for measurement of the reference PN, and the scope. The proposed algorithms are applied to the sampled data from the scope.

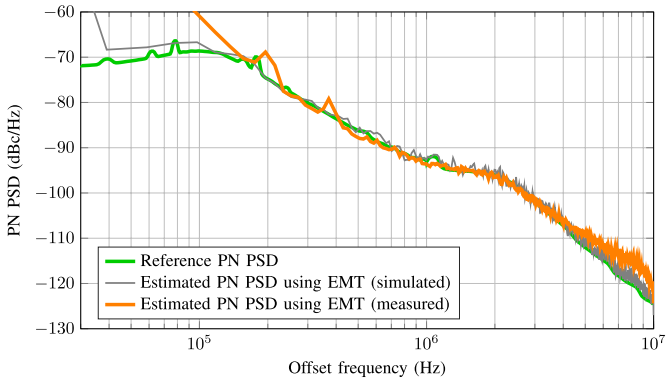

Fig. 11. Estimated and true PLL PN power spectrum (simulated and measured) using EMT. The PSD estimation is averaged over eight chirps.

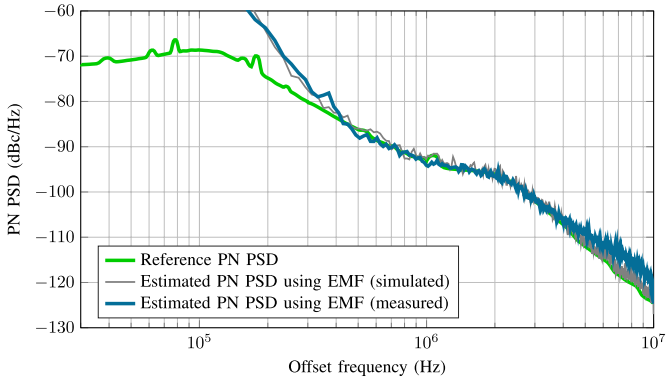

Fig. 12. Estimated and true PLL PN power spectrum (simulated and measured) using EMF. The PSD estimation is averaged over eight chirps.

average between the PN PSDs measured from CW signals at the carrier frequencies 11.8, 11.9, and 12.0 GHz with the spectrum analyzer. We observed that the PN slightly varied for these measurements, and thus, to provide a fair comparison, we averaged among all of them to obtain the reference. At this point, we would also like to highlight that our two estimation methods inherently deliver an average PSD of the PN over the entire bandwidth of the chirp.

B. Performance Analysis

The reference PN PSD and the resulting PN estimates for EMT and EMF are provided in Figs. 11 and 12, respectively. In each of the figures, the simulation and measurement results are compared. It is observed that for high frequencies, EMT and EMF (for both simulation and measurement) almost perfectly match the reference PN PSD. The individual mismatches are explained in the sequel.

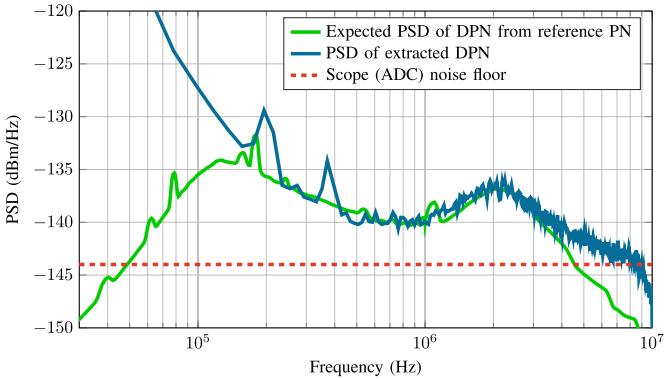

Fig. 13. Expected DPN PSD obtained from the reference PN, PSD of extracted DPN from the OCT IF signal, and scope (ADC) noise floor.

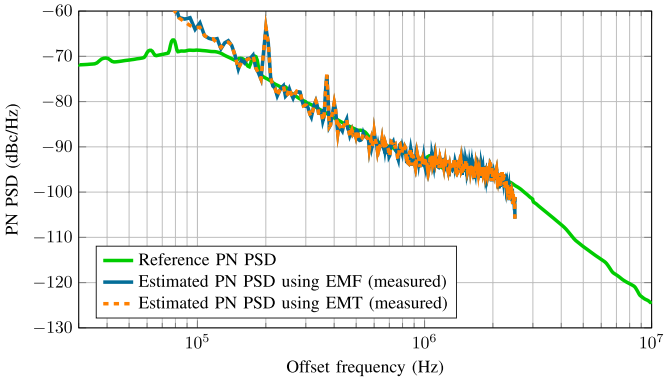

Fig. 14. Estimated and true PLL PN power spectrum (measured) using EMT and EMF. The sampling frequency of the OCT IF signal is reduced to $f_s = 5$ MHz, which allows for more accurate estimates at small offset frequencies.

First, it is important to mention that the measured OCT IF signal is far from a perfect sinusoidal due to hardware impairments. Thus, for both EMT and EMF, unavoidable estimation errors at small offset frequencies in the kilohertz range with comparably large amplitude occur. For the EMT, this can be observed intuitively by evaluating the DPN extraction in (18), as the subtracted cosine differs from $y_O[n]$. To clarify this further, we depict the PSD of the extracted DPN from the measured OCT IF signal $y_O[n]$, the expected DPN, and the scope noise floor in Fig. 13. The expected DPN is obtained according to (13) together with the (measured) reference PN PSD. For frequencies below 150 kHz, the expected and extracted DPN completely diverge due to the residual low frequency components. Obviously, this falsifies the PN estimates for small offset frequencies. Further interesting insights are revealed by comparing the estimates from the measured data to the simulation results. While the EMT from simulations achieves almost perfect estimation over the entire frequency range, the EMF performs worse for small offset frequencies. As mentioned already, this is due to the approximation in (25). Possibilities to improve this estimation will be presented in Section VIII-C.

For large offset frequencies in the MHz-range, it is observed that both EMT and EMF based on the simulations perfectly estimate the reference PN up to the cutoff frequency of the LPF. The estimates based on the measured data, however, deviate from the reference PN from 4 MHz upward. The reason for this is again delineated in Fig. 13. Therein, it is observed that for frequencies beyond 4 MHz, the expected DPN PSD is below the noise floor of the oscilloscope. Thus, for the estimation based on the measured data, both methods cannot recover the true PN for these offset frequencies.

From this analysis, it becomes clear that the DPN PSD highly depends on the PN of the PLL. Further, the OCT time delay and insertion loss severely affect the DPN extraction process. In this paper, we consider the noise floor of the signals in the analog domain, which is defined by the VCO output, the PA, and the mixer, to stay below the noise floor of the scope. By using the passive mixer in our hardware prototype, this is easily achieved. In [11], we show how to realize the OCT, such that the DPN extraction is optimized.

In conclusion, it is observed that EMT and EMF perform almost equivalently, except for small offset frequencies. Note, however, that the frequency axis is logarithmic in all the plots in this paper. On a linear frequency axis, it becomes clear that the differences between the algorithms are actually marginal. Still, since, specifically for PN PSDs, the values at low offset frequencies are of interest; we show how to improve the estimation at low-frequency offsets in the sequel.

C. Improvement of Estimation at Small Offset Frequencies

As mentioned already, the measured OCT IF signal is not perfectly sinusoidal. Thus, both EMT and EMF contain residual low frequency components with comparably large amplitude in the final estimates. These signal components could, of course, be eliminated with a high-pass filter. However, depending on the frequency response of this filter, the PN estimates would be falsified. We thus present a different approach to increase the resolution at small offset frequencies.

Through the windowing, which is carried out as part of the PSD estimation, these residual low frequencies are spread out in the frequency domain. In terms of shape, the used Hann window turned out to be a good choice for our method as it possesses a narrow main lobe. Thus, to notably reduce the windowing impact, the actual length of the window in absolute time is required to be increased. Obviously, this is achieved with a larger FFT, which is not desired as it leads to a massive complexity increase. Instead, we suggest to lower the sampling rate f_s, which also yields a longer window in absolute time.

To show the effectiveness of this countermeasure, we sampled the data from our hardware prototype with $f_s = 5$ MHz, which is a quarter of the 20 MHz used earlier on. Along with this, the main lobe of the Hann window becomes narrowed by a factor of 4, hence diminishing the impact of the unavoidable errors induced at low frequencies. The resulting PN estimates are shown in Fig. 14 for EMT and EMF. By comparing the results to Fig. 11 and Fig. 12, it is observed that the estimates now coincide with the reference PN down to 150 kHz. Further, EMF now achieves almost the same estimation result as EMT, as the approximation from (25) has less influence. Note that the peaks at 200 and 400 kHz, induced by impairments in our hardware setup, become more visible due to the higher frequency resolution.

TABLE III
COMPARISON TO EXISTING PN ESTIMATION TECHNIQUES

Approach	Input signal	Maximum input frequency	Offset frequency range	Ref. input	Core concept	Performance analysis
[3]	CW	n/a	100 Hz – 2 MHz	yes	All-digital ΣΔ-frequency discriminator	Comparison to simulated PN PSD
[4]	CW	2 GHz	100 kHz – 3.2 MHz	no	Voltage-controlled delay line with self-calibration	Single-tone sensitivity at 100 kHz offset: −124 dBc/Hz
[5]	CW	2 GHz	500 kHz – 12 MHz	no	Digital phase frequency detector, programmable charge pump	12.7% error over entire frequency range
[6]	CW	6 GHz	400 Hz – 1 MHz	no	In-phase/quadrature PN detection with self-calibration	Comparison to measured reference PN PSD
EMT (this work)	Linear FMCW	12 GHz (B = 200 MHz)	150 kHz – 4 MHz	no	Artificial on-chip target, signal processing in time domain	2.4% error over entire frequency range
EMF (this work)	Linear FMCW	12 GHz (B = 200 MHz)	150 kHz – 4 MHz	no	Artificial on-chip target, signal processing in frequency domain	3.5% error over entire frequency range

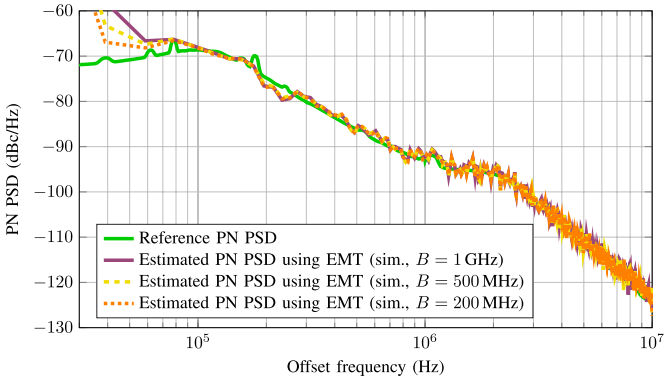

Fig. 15. Estimated and true PLL PN power spectrum using EMT (simulated) for various chirp bandwidths.

Clearly, this simple, yet effective countermeasure of reducing the sampling frequency also has a drawback. Since the estimation is possible only up to $f_s/2$, the measurement range is reduced. However, as altering the sampling frequency in a real-world application is easy, the PN can be successively obtained first for low offset frequencies (small f_s), and subsequently for high offset frequencies (large f_s).

D. PN Estimation for Higher Bandwidths

Up to here, the PN estimation has been carried out for a fixed bandwidth of $B = 200$ MHz only. However, the proposed PN estimation can be applied to higher bandwidths as well. This is shown in Fig. 15 for EMT based on simulations for chirp bandwidths of $B = 200$ MHz, $B = 500$ MHz, and $B = 1$ GHz. For each of the configurations, we optimized the OCT parameters according to [11]. It is observed that the PN estimates almost perfectly coincide for all bandwidths, and there are solely small deviations at the first three discrete frequency bins. Overall, however, the reference PN PSD is matched very well for all used bandwidths.

IX. DISCUSSION

To the best of our knowledge, the proposed methods are the first known solutions, enabling PN estimation from a linear FMCW signal. Although existing works presenting on-chip PN estimation techniques most commonly consider a CW input signal, we briefly carry out a comparison to such.

In Table III, an overview of existing work [3]–[6] is provided together with our proposed methods. It can be deduced that EMT and EMF exceed existing work with respect to the maximum frequency, and are able to estimate PN in similar offset frequency ranges. As for most of the others, no reference input is required. For performance comparison, we take up the idea from [5], and compute the relative error to the reference PN. In particular, we determined such by first averaging over individual PN estimates from eight chirps for each discrete frequency bin. The resulting errors are then averaged over all these bins for the frequency range given in Table III. Based on the measurements, both EMT and EMF feature an excellent average error of 2.4% and 3.5%, respectively.

X. CONCLUSION

In this paper, two concepts to obtain the PN power spectrum from a linear FMCW input signal are presented. We put emphasis on efficient realizations of the concepts in digital hardware and compared their computational complexity. Simulation and measurement results show that EMT, computed mainly in time domain, reveals excellent estimation performance at the cost of slightly higher complexity. Conversely, EMF, carried out mainly in frequency domain, persuades with lower computational effort at the cost of a slightly worse estimation performance for low offset frequencies. Both concepts enable PN estimation simultaneously to normal operation of an FMCW radar transceiver.

REFERENCES

[1] A. Melzer, A. Onic, and M. Huemer, "On the sensitivity degradation caused by short-range leakage in FMCW radar systems," in *Lecture Notes in Computer Science (LNCS): Computer Aided Systems Theory (EUROCAST 2015)*. Switzerland: Springer Int., 2015, pp. 513–520.

[2] K. Thurn, R. Ebelt, and M. Vossiek, "Noise in homodyne FMCW radar systems and its effects on ranging precision," in *IEEE MTT-S Int. Microw. Symp. Dig.*, Jun. 2013, pp. 1–3.

[3] M. Ouda, E. Hegazi, and H. F. Ragai, "Digital on-chip phase noise measurement," in *Proc. 4th Int. Design Test Workshop (IDT)*, Nov. 2009, pp. 1–5.

[4] W. Khalil, B. Bakkaloglu, and S. Kiaei, "A self-calibrated on-chip phase-noise measurement circuit with −75 dBc single-tone sensitivity at 100 kHz offset," *IEEE J. Solid-State Circuits*, vol. 42, no. 12, pp. 2758–2765, Dec. 2007.
[5] M. Ishida *et al.*, "A programmable on-chip picosecond jitter-measurement circuit without a reference-clock input," in *IEEE Int. Solid-State Circuits Conf. Dig. Tech. Papers (ISSCC)*, Feb. 2005, pp. 512–614.
[6] H. Gheidi and A. Banai, "Phase-noise measurement of microwave oscillators using phase-shifterless delay-line discriminator," *IEEE Trans. Microw. Theory Techn.*, vol. 58, no. 2, pp. 468–477, Feb. 2010.
[7] P. Mathecken, T. Riihonen, S. Werner, and R. Wichman, "Phase noise estimation in OFDM: Utilizing its associated spectral geometry," *IEEE Trans. Signal Process.*, vol. 64, no. 8, pp. 1999–2012, Apr. 2016.
[8] K. Harada, "Nonparametric spectral estimation of phase noise in modulated signals based on complementary autocorrelation," *IEEE Trans. Signal Process.*, vol. 62, no. 17, pp. 4479–4489, Sep. 2014.
[9] A. Melzer, A. Onic, F. Starzer, and M. Huemer, "Short-range leakage cancelation in FMCW radar transceivers using an artificial on-chip target," *IEEE J. Sel. Topics Signal Process.*, vol. 9, no. 8, pp. 1650–1660, Dec. 2015.
[10] A. Melzer, A. Onic, and M. Huemer, "Phase noise estimation in FMCW radar transceivers using an artificial on-chip target," in *IEEE MTT-S Int. Microw. Symp. Dig.*, San Francisco, CA, USA, May 2016, pp. 1–4.
[11] A. Melzer, F. Starzer, H. Jäger, and M. Huemer, "On-chip delay line for extraction of decorrelated phase noise in FMCW radar transceiver MMICs," in *Proc. 23rd Austrian Workshop Microelectron. (Austrochip)*, Vienna, Austria, Sep. 2015, pp. 31–35.
[12] M. C. Budge and M. P. Burt, "Range correlation effects in radars," in *Proc. Rec. IEEE Nat. Radar Conf.*, Apr. 1993, pp. 212–216.
[13] A. Papoulis and S. U. Pillai, *Probability, Random Variables and Stochastic Processes*. New York, NY, USA: McGraw-Hill, 2002.
[14] W. Gardner, "Common pitfalls in the application of stationary process theory to time-sampled and modulated signals," *IEEE Trans. Commun.*, vol. 35, no. 5, pp. 529–534, May 1987.
[15] P. Vary and R. Martin, *Digital Speech Transmission: Enhancement, Coding and Error Concealment*. Hoboken, NJ, USA: Wiley, Jan. 2006.
[16] F. J. Harris, "On the use of windows for harmonic analysis with the discrete Fourier transform," *Proc. IEEE*, vol. 66, no. 1, pp. 51–83, Jan. 1978.

Alexander Melzer (GS'14) was born in Voitsberg, Austria, in 1988. He received the Dipl.Ing. degree in telematics from the Graz University of Technology, Graz, Austria, in 2012. He is currently pursuing the Ph.D. degree in cooperation with Danube Integrated Circuit Engineering GmbH & Co., KG, Linz, Austria.

From 2013 to 2014, he was with Maxim Integrated Austria. Since 2014, he has been a member of the Institute of Signal Processing, Johannes Kepler University Linz, Linz. His current research interests include digital signal processing for automotive radar systems.

Alexander Onic (GS'07–M'13) received the Dipl.Ing. degree in electrical engineering (with a focus on information technology and signal processing) from the Friedrich-Alexander-Universität Erlangen–Nürnberg, Erlangen, Germany, in 2007, and the Ph.D. degree from Alpen-Adria-Universität Klagenfurt, Klagenfurt, Austria, in 2013.

While with Alpen-Adria-Universität Klagenfurt, in 2013, he was part of the research team that invented Unique Word OFDM, a novel signaling scheme for digital communication, under the supervision of Mario Huemer. He is currently a Concept Engineer with Automotive Radar, Infineon Technologies, Linz, Austria. His current research interests include signal processing, communication engineering, and estimation theory, which are consequently supplemented by the research cooperation of Infineon and Johannes-Kepler-Universität Linz, Linz, on radar signal processing.

Mario Huemer (SM'07) was born in Wels, Austria, in 1970. He received the Dipl.Ing. degree in mechatronics and the Dr.techn. (Ph.D.) degree from the Johannes Kepler University (JKU) Linz, Linz, Austria, in 1996 and 1999, respectively.

From 1997 to 2000, he was a Research Assistant with the Institute for Communications and Information Engineering, University of Linz, Linz. From 2000 to 2002, he was with the Research and Development Center for Wireless Products, Danube Integrated Circuit Engineering GmbH & Co., KG, Linz. From 2002 to 2004, he was a Lecturer with the University of Applied Sciences, Upper Austria, and from 2004 to 2007, he was an Associate Professor of electronics engineering with the University of Erlangen–Nuremberg, Erlangen, Germany. In 2007, he moved to Klagenfurt, Austria, to establish the Chair of Embedded Systems and Signal Processing with Klagenfurt University Klagenfurt, Austria, as a Full Professor. From 2012 to 2013, he served as the Dean with the Faculty of Technical Sciences. Since 2013, he has been the Head of the newly founded Institute of Signal Processing, JKU. His current research interests include statistical and adaptive signal processing, signal processing architectures and implementations, and also mixed signal processing with applications in information and communications engineering, radio frequency and baseband integrated circuits, and sensor and biomedical signal processing. Within these fields, he published over 190 papers.

Dr. Huemer was the recipient of dissertation awards of the German Society of Information Technology (ITG) and the Austrian Society of Information and Communication Technology in 2000, the Austrian Kardinal Innitzer Award in Natural Sciences in 2010, and the German ITG Award in 2016. His review work includes National and European Research projects and also international journals. From 2009 to 2015, he was a member of the Editorial Board of the *International Journal of Electronics and Communications*. He is a member of the IEEE Signal Processing Society, the IEEE Circuits and Systems Society, the IEEE Communications Society, and the IEEE Microwave Theory and Techniques Society. He is also a member of ITG and the Austrian Electrotechnical Association.